

# **Analysis of temporal and spatial dynamics of groundwater flow near groundwater abstraction sites**

**Sjoerd Polder**

**March 2025**

**MSc thesis**

**Hydrology and Environmental Hydraulics**

**Wageningen University**



# Abstract

Reliably estimating groundwater fluxes near groundwater abstraction sites is important for sustainable groundwater management. One approach to estimate these fluxes is through the analysis of temperature-depth profiles (TDPs) at deep (>50m) boreholes. This approach assumes that the temperature field will stabilise within 50 years, as indicated by some observations. In this study, the validity and impact of this assumption is tested. A combination of repeated TDPs, recorded in 2016/2018, 2023 and 2024 are compared to a conceptual transient 3D model to investigate the non-stationarity of temperature-depth profiles. Results show that TDPs are a valuable tool to estimate the vertical fluxes over an aquitard. However, while temperature profiles seem stable after 50 years, the model shows an underestimation of vertical fluxes, even after 180 years. The stabilization and accuracy are dependent on the flow rate over and thickness of the aquitard, where an increased flow rate and decreased aquitard thickness both increase accuracy. This study furthermore highlights the effect of climate change on the interpretation of TDPs and problems for interpretation when the aquitard of interest is relatively shallow (<50 m). These results highlight, on the one hand, some limitations in accurately determining groundwater fluxes near groundwater abstraction sites, but at the same time emphasize the importance of continuing temperature measurements to provide a temporal image of temperature-depth profiles and continue to improve understanding of the stability and accuracy of inferring vertical groundwater flow from TDPs.



# Contents

|       |   |    |
|-------|---|----|
| 1     | Introduction                                    | 1  |
| 1.1   | Research questions                              | 2  |
| 2     | Hydrogeology of field sites                     | 3  |
| 2.1   | Herveldse veld                                  | 3  |
| 2.2   | La Cabine                                       | 3  |
| 2.3   | Lower Rhine Embayment                           | 3  |
| 2.4   | Groundwater abstraction                         | 3  |
| 3     | Methods   | 7  |
| 3.1   | Temperature depth profiling                     | 7  |
| 3.1.1 | Bredehoeft and Papadopulos                      | 7  |
| 3.2   | Conceptual heat transport model                 | 8  |
| 3.2.1 | Model setup                                     | 8  |
| 3.2.2 | Data interpretation                             | 8  |
| 3.2.3 | Flow rates and accuracy                         | 9  |
| 4     | Results   | 11 |
| 4.1   | Temperature profiles                            | 11 |
| 4.1.1 | TDP's and temperature gradients                 | 11 |
| 4.1.2 | Differences                                     | 11 |
| 4.1.3 | Injection point                                 | 11 |
| 4.1.4 | Flow rates La Cabine                            | 12 |
| 4.2   | Model   | 13 |
| 4.2.1 | Temperature depth profiles and injection points | 13 |
| 4.2.2 | Flow rates                                      | 13 |
| 4.2.3 | Model variation                                 | 15 |
| 5     | Discussion                                      | 19 |
| 5.1   | Field data                                      | 19 |
| 5.2   | Model and comparison of field data and model    | 20 |
| 6     | Conclusion                                      | 23 |
|       | Acknowledgements                                | 25 |
| 6.1   | Artificial intelligence                         | 25 |
|       | Bibliography                                    | 27 |
| A     | Additional figures                              | 31 |



# 1 | Introduction

Groundwater is a vital source of drinking water, with more than 2.5 million people worldwide relying on groundwater (Shaji et al., 2021). In the Netherlands, 60 percent of all drinking water comes from groundwater sources (van Driezum et al., 2020). Groundwater has multiple advantages over surface water. Groundwater is naturally cleaner due to its natural filtration through the soil, which reduces pathogens and contaminants, resulting in lower risks of waterborne diseases compared to surface water sources (Hug et al., 2020). Furthermore, groundwater is available in many places where surface water is not available or is available only limited (Shaji et al., 2021).

However, according to van Driezum et al. (2020) more than half of the drinking water supplies in the Netherlands face problems, currently or in the near future. These problems are related to water quality and/or water quantity (van Driezum et al., 2020). Groundwater quality can be influenced by natural contaminants in the soil and anthropogenic sources (e.g. Hug et al. (2020) and J B and Joseph (2023)). These pollutants can potentially be problematic for drinking water (van Driezum et al., 2020).

The availability of groundwater is further negatively influenced by climate change, causing groundwater levels to drop globally (Wada et al., 2010). Furthermore, groundwater is over-abstracted (Wada et al., 2010). Problems with over abstraction are also present in a low-lying country as the Netherlands, where average groundwater levels are near the surface (Lijzen et al., 2014). To prevent groundwater over-abstraction, and utilize the groundwater abstraction stations optimally, the hydrogeological properties of the area are crucial to understand (Bierkens & Wada, 2019). In systems with shallow aquifers, it is proven difficult to estimate hydraulic properties (Bense et al., 2022; Scanlon et al., 2006). Especially when groundwater abstraction stations are active, flow across different aquitards can be difficult to quantify.

Groundwater abstraction can be done in an unconfined and confined aquifer. A confined aquifer has the advantage of being naturally filtered by soil and an aquitard above, preventing anthropogenic sources from entering the groundwater abstraction (J B & Joseph, 2023). However, confined aquifers can also have groundwater infiltration from potentially contaminated uncon-

ned aquifers (Pradhan et al., 2023). To estimate how large these fluxes inside an abstracted confined aquifer are, groundwater source and fluxes needs to be determined.

Currently, groundwater origin is determined by groundwater age, the time groundwater is in the soil since recharge. This can be estimated by sampling water, and applying various methods in the lab to obtain geochemical characteristics (Broers et al., 2021; Jasechko, 2019). These geochemical characteristics are generally used to divide groundwater into two binary categories. Either young groundwater (<50 years) or old groundwater (Thaw et al., 2022). Using this division, water categorised as young groundwater is prone to anthropogenic pollution.

While this method gives advantages for a clear distinction between possible contaminated water and water free from anthropogenic sources, it also has some drawbacks. This method requires samples from multiple depths to be taken and analysed in the lab, which is costly and only gives an image of one specific moment in time (Kurylyk et al., 2019). Another method for understanding groundwater age and flow, and infer hydrogeological properties is using temperature depth profiles (TDP's) (Bense et al., 2008; Bense et al., 2017; Kurylyk et al., 2019). Here the temperature is measured in a piezometer over the whole depth. Combining hydrogeological properties found in the borehole and the curvature of the temperature profile over that depth, the flow rate can be inferred (Bredehoeft & Papadopoulos, 1965). This method is widely used in the analysis of TDP's (e.g. Bense et al. (2020) and Bense et al. (2017)). For this method, the assumption is made that the temperature profile is relatively stable over time. While this is proven useful (Bense et al., 2017), there are questions about the usability near recent groundwater abstractions. Due to groundwater abstractions, groundwater flow can be altered. Heat flow stabilization needs to take place, which can potentially be much slower (Casillas-Trasvina et al., 2022). This is further influenced by climate change, causing surface warming impacting classical profile interpretation of TDPs (Kurylyk & MacQuarrie, 2014; Taniguchi et al., 1999). This can potentially influence the accuracy of estimating the vertical groundwater flux with the Bredehoeft and Papadopoulos method.

Bense et al. (2022) and Bense et al., 2017, looked at multiple temperature-depth profiles over time. In those analyses, uses in action points caused by surface warming to understand groundwater flow. However, next to these methods the assumption is made that Bredehoeft and Papadopulos can be applied near groundwater abstraction sites, since the situation seems relatively stable. However, it has not been studied how much time is needed for a system to stabilize after large changes, such as the start of groundwater abstractions. Furthermore, previous studies did not simulate heat flow in a transient 3D environment to study both the temporal and spatial components of groundwater flow near groundwater abstractions. This means the validity of the assumed stability for temperature-depth profiles near groundwater abstractions is not known. Therefore, the accuracy of the Bredehoeft and Papadopulos in an environment where groundwater is abstracted has never been studied and quantified before.

## 1.1 Research questions

This leads to the following research questions:

- ^ How accurately can groundwater flow through an aquitard be calculated with the Bredehoeft and Papadopulos method situated near a groundwater abstraction site?
  - How long does it take for groundwater coupled heat flow to stabilize during groundwater abstraction?
  - How can the stability of groundwater coupled heat flow be observed in temperature-depth profiles?
  - How accurate can groundwater fluxes be estimated based on a conceptual transient 3D model in relation to abstraction time?
  - How does surface warming impact the accuracy of the Bredehoeft and Papadopulos method?

## 2 | Hydrogeology of field sites

In this study field data from three different locations are studied, both from the Netherlands and Germany. At all sites groundwater is abstracted in a confined aquifer, but the subsurface, rate of abstraction and age of the groundwater abstraction are different. In figure 2.1 the 3 different locations are indicated.

### 2.1 Herveldse veld

The first location is in the Betuwe, located between the river Rhine and the Waal and close to the town of Zetten, the Netherlands. The top layer contains Holocene sediments from the river, varying from sandy clay to clay. Below these first meters, a sandy layer is present up to 15 meters depth. Subsequently, a layer of 15 meters of clay is present. From 40 to 70 meters depth the second sandy layer is present, with another clay layer beneath (TNO, 2024). This can be seen in figure 2.2

In the second sandy layer, groundwater has been abstracted since 2007. Due to the protection of the clay layer above this aquifer, this abstraction is seen as a non-phreatic abstraction. The abstraction rate since the start is relatively stable with rates between 3.5 and 4  $10^6 \text{ m}^3/\text{y}$  (Folmer et al., 2018a).

### 2.2 La Cabine

The second location is an area northwest of Arnhem, the Netherlands. It is on the bank of the Veluwe. The Veluwe is the largest push moraine complex in the Netherlands, where most of the area is semi-natural vegetation and forested. The subsurface contains subsequently glacial sands and gravels up to 50 meters depth, and riverine sands and gravels from 65 to 100 meters, with a clay layer beneath, creating a layered system with multiple aquifers and aquitards (Bense et al., 2022; TNO, 2024). This is illustrated in figure 2.2. The clay layers in this area are relatively thin, especially northeast of the groundwater abstraction (TNO, 2024).

In this forested area, there is the La Cabine Groundwater abstraction site (LC). At this site, groundwater has been abstracted since the 1910's. Since the 1970's, the abstraction rate is stable at around 9 to 10  $10^6 \text{ m}^3/\text{y}$  (Folmer et al., 2018b). While seasonal variation is not reported, inter-annual variations in abstraction rate are

limited. The abstraction in this area is in the aquifer between 70 and 90 meters depth. Due to the protection of the clay layer above this aquifer, this abstraction is seen as a non-phreatic abstraction.

### 2.3 Lower Rhine Embayment

The third area of interest is the Lower Rhine Embayment (LRE), Germany. The LRE is part of the Roer Valley Rift System, which is a southward extension of the North Sea Basin (Bense et al., 2008; Schäfer et al., 1996). This basin is filled with Oligocene sediments, containing predominately sands. Above these sandy sediments are younger sediments, containing both clay and sand layers. In between these younger sediment layers, layers of lignite are present (Schäfer et al., 1996). Figure 2.2 C provides a simplified interpretation of the subsurface.

In this region, the lignite is mined through open pit mining (Carmen, 2022; RWE, n.d.). These open pit lignite operations reach a depth of more than 300 meters deep. These mining operations started around the 1960s (RWE, n.d.). In order to allow these mining operations, groundwater needs to be abstracted on a large scale. Due to these large-scale groundwater abstractions, the hydraulic heads in this region show a large cone of depression near these mines (Bense & Van Balen, 2004). The scale and depth of this cone of depressions indicate that the groundwater abstraction rate is much larger than in the previous areas, but exact numbers are not publicly available.

In this area, there are many faults present. This alters groundwater flow significantly, since groundwater cannot flow freely through the aquifers (Schäfer et al., 1996). However, there are still clear effects of the groundwater abstractions seen at the other side of the fault, since a fault is not a complete block to flow but also allows for preferential flow paths along the fault plane (Bense et al., 2008; Gumm et al., 2016).

### 2.4 Groundwater abstraction

In all three regions described above, groundwater is abstracted in a confined aquifer. Although hydrogeological properties are different at each location, at all locations groundwater is abstracted in a confined aquifer, making groundwater fluxes over the different aquitards compa-

Figure 2.1: Map indicating the three different areas from where data is used in this study. The points are located in the area of interest, not at the specific boreholes used in this study. Both maps in this figure have the same scale.

table. The principles of groundwater and heat flow with groundwater abstraction in a confined aquifer are indicated in figure 2.3. Here flow lines are indicated for groundwater flow induced by the groundwater abstraction, given that there is no other preferential groundwater flow in the area. In figure 2.4, corresponding temperature lines are indicated. This illustration indicates that cold temperature from the surface near groundwater abstraction sites move more downward, while warm temperatures from below the groundwater abstraction moves upward, coupled to the groundwater flow.

Figure 2.2: Schematic interpretation of the borehole profiles at or near the groundwater abstraction sites. Interpretations are based on BRO REGIS hydrogeological interpretations from TNO (2024) and borehole descriptions near the abstraction sites.

Figure 2.3: Schematic overview of groundwater flow lines near groundwater abstraction in a confined aquifer

Figure 2.4: Schematic overview of temperature fields near groundwater abstraction in a confined aquifer, excluding surface warming. Lines of equal temperatures are displayed, indicating colder temperatures in the upper aquifer near the groundwater abstraction and warmer temperatures in the deeper aquifer.



## 3 | Methods

In this study, a combination of both real-world temperature-depth profiles, as well as a modelled heat transport over time are used. By comparing both physical data with a conceptual model, the (non-)stationarity of temperature-depth profiles near groundwater abstraction sites is studied.

### 3.1 Temperature depth profiling

Geothermal data is used from piezometers at 3 different sites, indicated in figure 2.1. At all locations, data is present from different years. Having measurements of multiple years allowed to investigate the stability of the profile, as well as The piezometers are PVC pipes, with a diameter of around 5 cm. This diameter is sufficiently narrow to prevent the profile from being disturbed by convective effects, as long as the temperature gradients in the well don't exceed  $0.1^{\circ}\text{C m}^{-1}$  (Bense et al., 2008). For all these piezometers, there is a detailed geological description available.

For the temperature-depth measurements, an autonomously logging thermometer (RBR SoloT logger, RBR Technologies Inc., Canada) is used. This thermometer has an accuracy of  $\pm 0.002$  K. The data will be collected with the stop-go methodology with intervals of 1 metre depth and 10 seconds. (Harris & Chapman, 2007). All measurements use the RBR SoloT logger, except for the measurements in the LRE in 2007. Here the In-Situ Inc. thermometer, a temperature probe with an accuracy of 0.01 K and a response time of 30 seconds is used. The depth interval of these measurements is 2 metres.

At the Herveldse veld one piezometer is sampled, since in this area there is only one piezometer that reaches the depth of the groundwater abstraction (TNO, 2024). This piezometer, piezometer B39F0836, is sampled in 2018, 2023 and 2024. At La Cabine, data of 2 piezometers, piezometers B40A0549 and B40A0552, is used. Both piezometers are placed deeper than the pumping depth, allowing the effect of the groundwater abstraction on vertical groundwater flow to be studied. there are measurements from 2016 (only B40A0552) 2018(only B40A0549), 2023 and 2024 for these piezometers. In the LRE, only one piezometer is used (piezometer 80908 (or 148929 in the database of Bohrungen in NRW - GD NRW (n.d.)). This is the only piezometer

used, since other samples were not close an abstraction and/or not measured for multiple years. This piezometer is measured in 2007 (Bense et al., 2008) and 2017.

For all different measurement locations, the temperature-depth profiles of the different years are plotted per piezometer with detailed geological descriptions. This allowed distinguishing signals in the temperature profiles between geological signals and flow signals. Next to the profile itself, the temperature gradients over depth are also calculated as the difference between each depth interval. Furthermore, the difference over time is also quantified by creating a plot with the difference between the different years divided by the time (in years) between the different measurements. Herby characteristics of each profile are reported.

Furthermore, the inflection points of all TDPs are calculated. The inflection point is the depth at which the lowest temperature is measured in a TDP. This is an indicator for groundwater flow (Bense et al., 2017). For each piezometer the trend between the inflection points is calculated to investigate the difference between abstraction sites over time.

#### 3.1.1 Bredehoeft and Papadopulos

Furthermore, quantification of flow across different layers are made with the Bredehoeft and Papadopulos formula (Bredehoeft & Papadopulos, 1965). Here the vertical flow velocity is calculated by the gradients within sections of the temperature profiles. These temperature gradients over a larger layer allows quantifying the flow within a specific geological layer. To do this, the value for the curvature needs to be found. The curvature over the aquitard is defined by equation 3.1. In this equation,  $Pe$  is the Peclet number, which is the indication of the curvature.  $Z$  is the depth from the top of the aquitard,  $T_0$  is the temperature at the top of the aquitard, and  $T_L$  is the temperature at the bottom of the aquitard.  $L$  is the thickness of the aquitard. This equation is solved numerically by iteration using the `fminsearch` function in MATLAB.

$$\frac{T - T_0}{T_L - T_0} = \frac{\exp\left(-\frac{Z - Z_0}{L}\right) - 1}{\exp\left(-\frac{L}{L}\right) - 1} \quad (3.1)$$

For calculating the flux from this Peclet number, equation 3.2 is needed (Bredehoeft & Papadopulos, 1965).

|             | Clay | Sand |
|-------------|------|------|
| k[m/d]      | 0.2  | 10   |
| kt[w/m/ °C] | 1.5  | 3    |

Table 3.1: values for hydraulic conductivity (k) and thermal conductivity (kt)

Figure 3.1: Geological description of different hydrogeological units used in the model. There are 3 aquifers indicated as sand and 2 aquitards indicated as clay.

$$Q_z = \frac{kt}{L C_p w} \quad (3.2)$$

The Bredehoeft equation is only applied for profile B40A0552, since other profiles don't have a clear thick aquitard to apply this method.

### 3.2 Conceptual heat transport model

In order to evaluate the effects of large groundwater abstractions on temperature profiles regionally, heat transport is modelled. A conceptual numerical 3D model is used with 3 different aquifers separated by 2 distinct aquitards. This model does not exactly match one of the sites where field data is available, but it is used to improve the understanding and interpretations of temperature-depth profiles. To solve the heat transport equation, as described in Bredehoeft and Papadopoulos (1965), a generic finite element code was used (Solutions, n.d.).

#### 3.2.1 Model setup

In figure 3.1, a 2D schematization of the simulated geology applied in the model is shown. The model is up to 750 metres depth, with the first and third aquifers 200 metres thick, and the middle aquifer 250 metres thick. The aquitards are 50 metres depth. The length and width of the model are 20 by 20 kilometres.

For the heat capacity and hydraulic properties, generic values for sand (aquifer) and clay (aquitard) are chosen based upon Bense et al. (2020) and Witte et

al. (2002), see table 3.1. In this model, there is the assumption of isotropy, so vertical and horizontal hydraulic conductivity are equal. At the top of the model, the surface, a continuous rain flux of 0.25 mm/day is applied. At one edge, across the whole vertical domain, a drain is applied as a Dirichlet boundary, with a head value of -5 m. All other edges have a Neumann no-flow boundary.

In this model, groundwater abstraction is enabled after 20 years by lowering the head in the middle aquifer, in a circle with a 200 meter radius from the centre of the model, to -2.5 m. Running the model without groundwater abstraction indicated a head in this area of around -0.5 m, effectively lowering the head near the groundwater abstraction 2 metres.

Surface warming is included as a constant, with a surface temperature of 9.1°C and increasing 0.02 K per year. At the bottom of the model, at 750 meters depth, a constant warming of 0.05 K m<sup>-1</sup> is added to simulate the geothermal heat flux (Bense et al., 2008).

$$c \frac{T}{t} + c_w \frac{1}{w} q_r T - r^2 T = 0 \quad (3.3)$$

Transient heat transfer by advection through groundwater flow and conduction in a saturated porous medium is described by equation 3.3, in which  $v$  [m=s] is the Darcy velocity of groundwater flow,  $T$  is temperature (°C),  $c$  (2:0 · 10<sup>3</sup> j kg<sup>-1</sup>) °C<sup>-1</sup>) and  $c_w$  (4:2 · 10<sup>3</sup>kg<sup>-1</sup> °C<sup>-1</sup>) are the specific heat of the saturated sediment and water, respectively, ( $\rho_s$ : 2:1 · 10<sup>3</sup>kgm<sup>-3</sup>) and  $\rho_w$  (1 · 10<sup>3</sup>kgm<sup>-3</sup>) are their respective mass densities,  $k$  is the thermal conductivity [W m<sup>-1</sup> °C<sup>-1</sup>] of the saturated sediment (based upon Bense et al. (2008)).

To study the sensitivity of the parameters chosen, there are two variations made on the model. One run has a double head difference, increasing the head to -4 meters at the abstraction site to increase the groundwater flow over the aquitard. The other model run has halve the thickness for both aquitards.

#### 3.2.2 Data interpretation

From this 3D model several techniques are used. From the temperature field, several temperature profiles are

extracted and compared for their spatial and temporal evolution. This is done to see the distance the abstraction is affecting the TDPs and to what degree this is stationary.

From the temperature data, the injection points near the abstraction sites are also mapped with a 10-metre horizontal resolution and a 1-metre vertical resolution, according to the same method applied for injection point calculations at the measured TDPs.

### 3.2.3 Flow rates and accuracy

To investigate how accurate flow rates can be calculated using TDPs, the flow rate is calculated with the Bredehoeft and Papadopoulos method, described in section 3.1.1

The flow rate is compared to the flow rate the model indicates over the aquitard. Furthermore, the flow rate by the Bredehoeft formula is compared with different moments from the abstraction onwards, to see the temporal behaviour of the curvature, and therefore the calculated flow rates.

To indicate how accurate the calculated fluxes are, the accuracy of the are calculated with equation 3.4. In this equation  $T_v$  is the test value. This is the flux calculated with the Bredehoeft formula  $O_v$  is the original value. This is the flux extracted from the model.

$$\text{Accuracy} = 100 \cdot \frac{T_v - O_v}{T_v} \cdot 100 \quad (3.4)$$



## 4 | Results

### 4.1 Temperature profiles

#### 4.1.1 TDP's and temperature gradients

In figure 4.1, the physical temperature-depth profiles at Herveldse veld (A, B39F0836), La Cabine (B, B40A0549 and C, B40A0552), and the LRE (D, 80908) are plotted, combined with the corresponding temperature gradient profile. In figure 4.1 A, temperatures increased between 2018 and 2024 throughout the profile. The surface warming can be observed, with an increase at the top of almost 2°C compared to 40 metres depth. Temperature differences between the measurements are largest near the surface and between 60 and 80 metres depth where groundwater is abstracted. All measurements at this piezometer show limited interaction with the geological formations below 120 metres depth. In the corresponding figure 4.1 E, the temperature gradient is largest near the surface and in the layer where the groundwater is abstracted. Between the years, there is hardly any difference observed between the different measurements.

In figure 4.1 B, surface warming can also be observed. Up to 100 metres depth the profile has warmed up. From below 100 meters, there seems to be little to no difference between the different measurements. Furthermore, the effect of the different clay layers is hardly visible within this whole profile. Only the clay layer at 130 metres seems to have an effect, although this is not very significant. In the temperature gradients (4.1 F), there is a small increase from the surface to 150 metres depth.

In (4.1 C), the most striking detail is the clear increase in temperature from 85 to 110 meters depth, which is the layer where groundwater is abstracted. Surface warming can be seen in all profiles, with up to 80 meters showing a clear effect. Below the abstraction depths, the temperature also increased slightly. The temperature gradients in this profile (4.1 G) are not stable in the pumped layer, but are higher in the abstraction layer, with values up to 0.1°C m<sup>-1</sup>, while the rest of the profile is between -0.05°C m<sup>-1</sup> near the surface and 0.02°C m<sup>-1</sup> further away from the abstraction area, which is a value also seen in other profiles in non-abstraction zones.

Figure 4.1 D's most remarkable feature is near the

thick lignite layers near 150 and 200 metres. The gradients in these layers (4.1 H) reaches 0.3 m<sup>-1</sup>, which is higher than values seen in other profiles. In between the lignite, where groundwater is abstracted, and near the surface temperature are increased between measurements. Furthermore, temperatures within the profile are stable

#### 4.1.2 Differences

In figure 4.2, the differences between measurements per year are displayed. Most of the observed differences from 4.1 are also visible in this plot. Near the surface the temperature has the strongest increase. The abstraction layer is also clearly visible in this plot with an increased temperature difference. In figure 4.2 A, there is no significant difference in temperature increase per year between the different measurements.

In figure 4.2 B, it can be seen that deeper down the profile is cooling down. While the surface is warming continuously, last year there seems to be a small decrease in temperature over the years starting near/below abstraction depths.

Figure 4.2 C shows instability in the abstraction layer, especially when comparing 2024 with 2023 data. This plot confirms the more significant temperature increase above the groundwater abstraction zone compared to below the abstraction.

Figure 4.2 D also confirms patterns seen in 4.1 D with an increase in temperature at the surface and at the abstraction layer. However, the temperature increase in the abstraction layer in this profile is with 0.04°C y<sup>-1</sup> rather large in comparison to other profiles. Except for the surface warming, increases in most profiles are only limited to 0.02°C y<sup>-1</sup>, apart from the difference between 2023 and 2024 in the abstraction depth of figure 4.2 C.

#### 4.1.3 Inlection point

The inlection points vary largely between the different plots (figure 4.3). In figure 4.3 A the inlection point is between 35 and 40 with a clear trend downwards of 1.11 metres per year. Near La Cabine, the downward movement of the inlection point is much smaller, without a significant trend very close to the groundwater abstraction (figure 4.2 C) and 0.47 metres per year further away

Figure 4.1: Temperature depth profiles (A till D) and Temperature gradients (E till H) taken at different years. For each location, data of the borehole description is displayed in these plots.

Figure 4.2: Differences of temperature between measurements at 4 different boreholes. The temperature differences are expressed as degrees Celsius per year. For each location data of the borehole description is displayed in these plots.

from the groundwater abstraction (figure 4.2 B). However, the infiltration point is here deep, with 60 metres for piezometer B40A0549 and even around 80 metres for piezometer B40A0552. For piezometer 80908 in Germany (figure 4.2 D), there is a large increase of 2 metres per year. However, it should be noted that due to deep and slow groundwater levels, surface temperatures could not be measured.

#### 4.1.4 Flow rates La Cabine

For the aquitard between 105 and 120 metres in depth, the second aquitard in the system, the Bredehoeft curves and flow rates are calculated (figure 4.4). The curves in this figure indicate a clear flow upwards. There seems to be an increase in flow rate from 1987mm/y to 2522mm/y. However, the variation within the profile is quite large, and this increase is not very stable, as the increase is much larger between 2024 and 2023 in comparison to 2023 and 2016.

Figure 4.3: In ection point of each temperature depth measurement at four di erent boreholes. A trend line is added based on the average change in in ection point depth per year

K at 300 metres from the abstraction site ( gure 4.5 C).

Furthermore, the in ection point is increasing with time. With a decreased distance to the abstraction site, the in ection points reach deeper depths compared to further from the abstraction site. The trend in in ection point movement is displayed in gure 4.6. It can be seen that the in ection points near the abstraction site (300 metres from abstraction) are getting deeper with a higher rate of 1.09 metre per year. This rate decreases when getting further from the abstraction site. With 600 metres from abstraction the rate decreases to 0.87m per year, and at 1200 metres from the abstraction the rate is 0.71m per year. These calculated rates seem to slow down around 160 years. All in ection points at this point are above the trend line, indicating that the trend is slower here compared to the trend over the whole time range.

To get an overview of the change in infection point spatially, in gure 4.7 the in ection points are plotted near the abstraction zone. In 4.7 A the blue areas indicate deeper in ection points, and are present around the abstraction site. In the area around the blue, a trend with distance to the abstraction site is less clear. However, green is more prevalent near the abstraction compared to yellow, although the pattern contains quite some noise, making the e ect of the abstraction less clear.

Figure 4.4: Flow rate across aquitard calculated with the Bredehoeft method at piezometer B40A0552, for the measurements at 2016,2023 and 2024. A smoothened line is plotted combined with the points for the individual data points. Qz values in this plot are in meters per year.

In 4.7 B all in ection points are deeper. However, the deepening of the in ection point less than 100 meters from the abstraction are the most strong, with values up to 250 meters. Up to 800 meters from the abstraction area the depth in ection point is correlated to the distance to the abstraction, with being closer relates to a deeper in ection point. Further away from the abstraction site, there seems to be a limited e ect of the groundwater abstraction itself. In 4.7 C, the in ection points are deepened more compared to 4.7 B. Both near the abstraction area, but also further away from the abstraction site the e ect is visible. Up to 1300 meters there is a clear correlation with the abstraction site. Near the abstraction site, the in ection point depth is around 250 meters, but for a larger area than in subplot B. At the border of this plot, the in ection point reaches a depth of 180 metres.

## 4.2 Model

### 4.2.1 Temperature depth profiles and in ection points

In gure 4.5 modelled temperature-depth profiles with di erent distances to abstraction site are displayed. It can be seen that in the upper aquitard the temperature is becoming colder over time. This difference is most noticeable near the abstraction site, with a decrease of 0.55 K at 300 meter from the abstraction site ( gure 4.5 C). In the bottom aquitard an increase of temperature with increasing abstraction time can be observed. This is, similar to the upper aquitard, most noticeable near the abstraction site, with a temperature increase of 1.6

### 4.2.2 Flow rates

In gure 4.8, the Bredehoeft curves are plotted as a measure of the ow rate possible in the eld. In gure

Figure 4.5: Modelled temperature-depth profiles with injection points at different distances from abstraction site. Time from abstraction ranges from 0 to 180 years. Figure A is 1200 metres from abstraction, B is 600 metres from the abstraction site, and C is 300 metres from the abstraction site.

Figure 4.6: The depth of the modelled injection point over time. In yellow the injection points 300 metres from abstraction are shown, in red 600 metres and in blue 1200 metres.

(a) (b) (c)

Figure 4.7: In section points near abstraction zone 60, 120 and 160 years after abstraction is started in the model. The abstraction area is marked white, because the model was not able to calculate values here correctly. In each plot, the scale of the in section points is different since depth ranges are quite large between the plots.

4.8 A it can be seen that the curvatures are increasing accurate. This is in line with figure 4.8, where Brede- over time. The Peclet number is negative, indicating hoefft curves are not accurate from 140 years onward, ow downwards. Up to 120 years it follows the dot- causing unrealistic ow rates. ted lines with fixed Peclet number, resulting in a profile Flow over the deeper aquitard is more stable, and that allows the calculation of ow rates. From 140 years the accuracy for 300 and 600 meters from the abstrac- onwards the curves do not follow the reference curva- tion is steadily increasing until 180 years, the end of the ture lines anymore, indicating a possible problem with simulation. For both 300 and 600 meters the accuracy the calculation. In this case, this is caused by the in- reached over 60%. At 1200 meters from abstraction the accuracy is lower than for all other locations and depths. fection point being within the profile 4.5. The ow rate However, the ow rate at this location is signi cantly ranges from 90 mm/year after 4 years of abstraction to 551 mm/y after 120 years of abstraction with the same lower than near the other locations, with 15 mm/year of abstraction rate in the model. ow. This causes the relative error margin to be large

In figure 4.8 B, similar behaviour can be observed. while the absolute error is small. Peclet numbers increase over time. Positive Peclet num- 4.2.3 Model variation bers here indicate groundwater ow upwards. In the first 100 years the increase seems to have a steady pace, where this pace decreases later on, slowly reaching a stable level. Since these deep levels are not effected by theing the scenarios at the upper aquifer, it can be observed movement of the in section point, there are no measure- that an increase in head difference results in an increase ments that do not follow normal curves indicated by the in accuracy around 80 to 100 years. However, this ac- dashed lines. Before abstraction started, groundwater curacy drops after 120 years, caused by in fection points ow as downward as opposed to upward, causing val- moving into the aquitard. A decreased thickness of the ues at start of model not to be accurate. Exact for the aquitard leads to a strongly decreased time for reach- ow rate range from 2 mm/year downwards after 4 years ing accuracies over 80% within 60 years. However, the of abstraction to 330 mm/y upwards after 180 years of accuracy drops signi cantly after only 80 years. In con- abstraction with the same abstraction rate in the model. trast to the other scenarios, the in fection point didn't

Similar plots are made for locations 600 and 1200 reach the aquitard here yet, as can be seen in appendix meters from the abstraction site. These can be found in A.4. However, appendix A.7 shows that the Bredehoeft Appendix A.5 and A.6 curves after 80 years do not follow the reference curva- ture lines, indicating unreliable data.

The accuracy of the calculated fluxes are plotted in figure 4.9. All accuracies increase over time, until For the accuracy at the deeper aquitard, the differ- 140 years. After 120 years the accuracy increases to ences are less pronounced. However, with a decreased 90% for all different distances from abstraction. Further aquitard thickness, the accuracy is consistently higher away from the abstraction, the initial accuracy is higher, than the reference scenario, with a difference of 10 per- but the rate of improvement is slower. From 140 years centage points. For the scenario with the increased onwards, the fluxes at 200 meters become rapidly less head difference, the difference with the reference sce-

(a)

(b)

Figure 4.8: Bredehoeft curves for the shallow (figure A) and deep (figure B) aquitard at 300 meters from the abstraction site. The different times since abstraction are indicated with different colours.

Figure 4.9: The accuracy of the vertical groundwater flow in the model in relation to time since abstraction. The real flux indicated by the model is compared to the flux calculated with the Bredehoeft method. This is done for both the shallow and the deep aquitard. The distances from the abstraction site are 300,600, and 1200 metres.

Figure 4.10: Comparison of the accuracy of the calculated fluxes at 300 metres from the abstraction site. For the 3 scenarios the accuracy is calculated at the first and second aquitard.

nario slowly increases to a higher accuracy, with the accuracy reaching up to 75%, which is similar to the accuracy of the decreased aquitard thickness

The flow rate with the increased head differences is increased with a factor 2, both for the upper and lower aquitard. This results in flow rates of 1070 and 970 mm/y for respectively the upper and lower aquitard. For the decreased aquitard thickness, the flow rate over the aquitards is similar to a bit lower, with flow rates of 520 and 530 mm/y respectively.



## 5 | Discussion

### 5.1 Field data

Temperature profiles can have very different characteristics and indicators, depending on multiple factors. Local and regional geology is important, since clay limits groundwater flow and heat transport, often seen as a jump in temperatures (Witte et al., 2002). However, profiles plotted in figure 4.1 have different characteristics, even when the geology in certain layers is similar. In Herveldse veld and the LRE a clear instability, which cannot be observed at la Cabine.

Groundwater abstraction does influence groundwater flow in the pumped aquifer, but also in the aquifers above and below. This impacts TDPs in the area near abstraction sites, because heat transport is coupled to groundwater flow (Bense et al., 2020). Therefore changes in flow regime caused by groundwater abstraction will also be seen at TDPs, since water with a different temperature will flow in.

The rise of temperature in proximity of the abstraction depth at Herveldse veld and the LRE indicates warm water flowing in. This can either come from deeper groundwater moving up or a warmer lateral flow, since groundwater from above the abstraction depth is cooler. This change in temperatures is furthermore an indication of a non-stable temperature profile. This is in line with Ziagos and Blackwell (1986), where the combination of transport and a bulge shape in a profile indicates the non-stationarity in a profile.

This instability is also seen in the LRE, where even with abstractions since the 1970s, a more distinct bulge at abstraction depth is observed. Due to changing and unknown abstraction rates for the moving lignite mining, this area shows clear instability. This indicates that stability of a temperature profile is not only dependent on the time since abstraction rate, but also on the geology, and the continuity and rate of groundwater abstraction.

The TDPs at Herveldse veld show a larger increase in the depth of the inflection point per year compared to La Cabine, as seen in figure 4.3. According to Bense et al. (2020), this can indicate an increased flux. This is in line with the groundwater abstraction being much more recent (Folmer et al., 2018a, 2018b), but at the same time leaves questions about the absolute flux. As the groundwater abstraction is 3 times smaller at Herveldse veld, this increased downward moving rate of inflection

point raises questions about the possibility of obtaining groundwater fluxes from inflection points alone.

At La Cabine, profile B40A0549 in figure 4.2 seems to indicate some limited cooling at the bottom, although not clear. This can either be a depth problem (depth not recorded correctly), or a result. Since there are no other signs of depth problems, this signal may be connected to groundwater flow (Witte et al., 2002). However, since this can only be seen in one measurement at one of the locations near La Cabine, conclusions cannot be made here. This confirms the importance of continuing the efforts to create an elaborative dataset with TDPs measured over multiple years.

For B40A0552, closest to the abstraction itself, it can be observed that there is a large temperature increase at the depth of the temperature. While this is a different signal than other profiles have, this can be seen as an indication of groundwater abstraction as well. While the difference plot looks quite chaotic for comparing 2024 with 2023, there seems to be a relatively stable situation here. Large temperature changes mainly occur near the surface, caused by surface warming.

While both profiles at La Cabine are different, there is no indication of instability in these temperature profiles, other than the expected surface warming. This stability allows applying the Bredehoeft and Papadopoulos equation to calculate vertical fluxes based on the temperature profile (Bredehoeft & Papadopoulos, 1965). There is some variation in groundwater fluxes calculated, as seen in figure 4.4. However, these variations are not linear over time, since the difference between 2023 and 2024 is larger than the difference between 2016 and 2023. This seems to indicate that this difference is less caused by a general trend and more by small measurement variations or groundwater flow variations. However, the flux is increasing between the measurements. To better understand the stability of calculation, the efforts of continuing the measurements in this area are of great importance to increase the significance.

One point of uncertainty for the calculation is the thickness of the clay layer, which is determined by the REGIS model of TNO (TNO, 2024) instead of the borehole description. This is done because the observed curvature in the profile exceeded the depth range of the clay layer in the borehole description. This causes the thickness and exact depth range of this aquitard to be

less precise. While this can influence the exact flux, the effect was limited for comparing the different profiles.

## 5.2 Model and comparison of field data and model

TDPs generated by the model are in line with the groundwater fluxes and head differences in the model. The surface warming and increased temperatures are seen in the field observations (figure 4.1). However, cooling is not widely observed. Only some limited cooling in profile B40A0552 for one observation. However, this cooling at different depths does occur at other field sites, as found by Bense et al. (2020).

Vertical groundwater flow is increased near the groundwater abstraction site. While groundwater abstraction can cause increased flow rates over an aquitard, there is a spatial relation between distance to the abstraction site and flux over the aquitard (Bense et al., 2022). This can be explained by the uniformity of the model, causing distance to the abstraction to be the only variable impacting flow, while studies with field data suggests variations in thickness of the aquitard and local/regional topography to be a larger driver (Bense et al., 2022). Rates of vertical groundwater flow are similar as found in real life.

The spatial map of the inflection points of the model showed some instability in the model, especially shortly after the abstraction starts in the model (figure 4.7). While inflection points movement is stable over time at the same location, there is some spatial variability that cannot be explained by the groundwater abstraction. While it is not completely clear why this happened, the effect on estimating trends is limited. Temperature-depth profiles from the model are comparable and the spatial variation is significantly smaller than the temporal variation.

The accuracy calculations of the fluxes in the model suggest a clear underestimation of the fluxes using the Bredehoeft and Papadopulos method. This is in contrast to previously made estimations, where the assumptions are made that TDPs are much quicker stabilised (e.g. Bense et al. (2022) and Bredehoeft and Papadopulos (1965)). It furthermore highlights the importance of checking the shape of the Bredehoeft curve, since calculations of the Peclet number cannot be done when the calculations are not done over a non-uniform curvature, such as happens when the inflection point reaches into the aquitard.

The model variations give an insight into the representability of the accuracies presented. While the trends were similar for all 3 scenarios, the exact accuracies can be quite different. Especially for the upper aquitard, effects of the scenarios in inflection points movement can be seen. This complicates the analysis of flow at the upper aquitard. However, comparing different years of measurements can give an indication of the stability of the profile, since no to limited increase in groundwater fluxes can be associated with general higher accuracies. At the lower aquitard, a more stable situation can be seen. The accuracy are in general similar. However, it can be seen that the accuracy improves with a decreased thickness of the aquitard and, in the long run, also with an increased flow rate. This indicates that depending on the local hydrogeology and abstraction accurate values can be seen earlier. This indicates the importance of the local and regional hydrogeology of the study area, since both groundwater fluxes and the thickness of the aquifer influence the accuracy of the calculated groundwater flux.

The setup of the model is not entirely comparable to situations seen at groundwater abstractions in the Netherlands. The model was developed for simulating groundwater flow near the lignite mines in the Lower Rhine Embayment, and converted to the Netherlands by adapting the soil parameters to clay instead of lignite values. However, the depth is still significantly larger than real life. While the relative thickness of the layers are comparable, the absolute thickness of each layer is approximately 5 times as large as seen in areas in the Netherlands, such as La Cabine. Although this can be a source of error, scaling methods for groundwater modelling are used often (Vermeulen et al., 2006; Wu et al., 2023).

Comparing the model results to the field observations results gives some discrepancies. While field observations suggest stabilization of heat flow within 50 years, the model suggests it takes significantly longer with a relatively stable situation near 140 years, if there are no problems with the inflection point moving into the aquitard. This can be caused by the scaling in this model. Furthermore, the groundwater flux in La Cabine is 4 times larger compared to the model. When groundwater flow is stronger, heat transport, and thereby stabilization of the temperature-depth profile can also occur quicker (Casillas-Trasvina et al., 2022). Furthermore, it is based on this dataset not yet certain if temperature profiles are completely stable, since there is some varia-

tion between the calculated fluxes, with the most recent measurement having the largest flux.



## 6 | Conclusion

Groundwater abstraction not only impacts groundwater flow itself, but also should be taken into account when analysing temperature-depth profiles. The model and the field observations confirm that effects of groundwater abstraction can be observed in temperature-depth profiles within 10 years of groundwater abstraction. Having observations over multiple years is crucial to understand temporal behaviour near groundwater abstraction.

Injection points can be a useful tool in understanding groundwater flow. Injection points can give a clear image of groundwater flow and the stability of temperature-depth profiles. However, differences in geology can limit the usability of this method, since the geology influences injection point movement.

The Bredehoeft and Papadopulos method is often applied to estimate flow over an aquitard. While this study shows that this method can be useful, the vertical flux tends to be underestimated. This underestimation is dependent on the time since abstraction, the distance from the abstraction site and the flux itself. According to the model, this method's accuracy is estimated to be below 40% after 20 years of abstraction to 75% after 140 years of abstraction. However, this can be influenced by the groundwater flux itself and the thickness of the aquitard, where an increased flow rate causes a higher accuracy after approximately 100 years, and a decreased aquitard thickness causes higher accuracies and quicker stabilization. Surface warming can become a problem for the usability of the Bredehoeft and Papadopulos method for relatively shallow aquitards. If the injection point moves into the aquitard, the method cannot be applied accurately anymore. This should be checked before applying this method to ensure its validity.

Interpreting TDPs and applying, where applicable, the Bredehoeft and Papadopulos method to field data suggests that temperature stability and thereby accurate usage of this method can be done within a shorter timespan. Observations indicate that after 17 years there has not been reached a steady-state. This can be seen because the TDPs have characteristics that indicate non-stationarity, such as a bulge at the depth of the abstraction. After approximately 50-60 years, the temperature-depth profile seems to be stable. Applying Bredehoeft here gives some variation in value, but there is no clear sign of an increase in the measured flux.

This study marks the importance of a good un-

derstanding of the temporal behaviour of temperature-depth profiles. After initial stabilisation, after 40-60 years, both the model and field observations show that groundwater flows can be estimated with the Bredehoeft and Papadopulos method to get an order of magnitude for the flow. For exact quantification, a more precise understanding of the temporal behaviour is needed. While the model used in this suggests that stabilization of TDPs takes more than a century, field data suggests a quicker stabilization of around 50 years. Continuing temperature-depth measurements near groundwater abstractions are crucial to better estimate the time stabilization a TDP takes from the start of the groundwater abstraction.



# Acknowledgements

Firstly, I want to thank Victor Bense for supervising this thesis, providing the temperature-depth data, testing and giving ideas about improvements for the model, and helping with restructuring this thesis when the original idea couldn't continue. This was crucial, since access needed for the measurements as part of the original ideas couldn't continue, leaving me with little inspiration at that moment. Without this help, this thesis could not have been done.

Furthermore, I want to thank Vitens water supply company for access to the boreholes in order to obtain the temperature-depth profiles. Lastly, I want to thank the students

Lastly, I want to thank students that followed the Advanced hydrogeology course in 2023 and 2024. With this course data was collected that was needed for this study.

## 6.1 Artificial intelligence

I used generative AI in this thesis. I mainly used ChatGPT for coding. Here I came up with code and code ideas, but used ChatGPT to fix some of the mistakes and helped filling in missing elements. I always checked codes for mistakes.

Furthermore, I used Grammarly to detect grammar mistakes in this thesis. All text is written by myself, but the spell check and some grammar mistakes detected by Grammarly are corrected. Grammarly used AI to detect grammar mistakes.

Lastly, I used Perplexity AI and SciSpace as an additional research tool for literature. Most research I found the traditional way, but some additional papers were found by AI. I always read the paper advised by AI, to study its content and confirm if the information I needed and expected from that paper is present.



# Bibliography

- Bense, V. F., Kruijssen, T., van der Ploeg, M. P., & Kurylyk, B. L. (2022). Inferring Aquitard Hydraulic Conductivity Using Transient Temperature-Depth Profiles Impacted by Ground Surface Warming. *Water Resources Research* 58(5), e2021WR030586. <https://doi.org/10.1029/2021WR030586>
- Bense, V. F., Kurylyk, B. L., de Bruin, J. G. H., & Visser, P. (2020). Repeated Subsurface Thermal Profiling to Reveal Temporal Variability in Deep Groundwater Flow Conditions. *Water Resources Research* 56(6), e2019WR026913. <https://doi.org/10.1029/2019WR026913>
- Bense, V. F., Person, M. A., Chaudhary, K., You, Y., Cremer, N., & Simon, S. (2008). Thermal anomalies indicate preferential flow along faults in unconsolidated sedimentary aquifers. *Geophysical Research Letters* 35(24). <https://doi.org/10.1029/2008GL036017>
- Bense, V. F., Kurylyk, B. L., van Daal, J., van der Ploeg, M. J., & Carey, S. K. (2017). Interpreting Repeated Temperature-Depth Profiles for Groundwater Flow. *Water Resources Research* 53(10), 8639–8647. <https://doi.org/10.1002/2017WR021496>
- Bense, V. F., & Van Balen, R. (2004). The effect of fault relay and clay smearing on groundwater flow patterns in the Lower Rhine Embayment. *Basin Research* 16(3), 397–411. <https://doi.org/10.1111/j.1365-2117.2004.00238.x>
- Bierkens, M. F. P., & Wada, Y. (2019). Non-renewable groundwater use and groundwater depletion: a review. *Environmental Research Letters* 14(6), 063002. <https://doi.org/10.1088/1748-9326/ab1a5f>
- Bohrungen in NRW - GD NRW(n.d.). Retrieved October 29, 2024, from <https://www.bohrungen.nrw.de/>
- Bredehoeft, J. D., & Papadopoulos, I. S. (1965). Rates of vertical groundwater movement estimated from the Earth's thermal profile. *Water Resources Research* 1(2), 325–328. <https://doi.org/10.1029/WR001i002p00325>
- Broers, H. P., Sültenfuß, J., Aeschbach, W., Kersting, A., Menkovich, A., de Weert, J., & Castelijn, J. (2021). Paleoclimate Signals and Groundwater Age Distributions From 39 Public Water Works in the Netherlands; Insights From Noble Gases and Carbon, Hydrogen and Oxygen Isotope Tracers. *Water Resources Research* 57(7), e2020WR029058. <https://doi.org/10.1029/2020WR029058>
- Carmen. (2022, June 3). The ten biggest surface mines in Europe [Mining technology]. Retrieved September 9, 2024, from <https://www.mining-technology.com/marketdata/ten-biggest-surface-mines-in-operation-in-europe/>
- Casillas-Trasvina, A., Rogiers, B., Beerten, K., Wouters, L., & Walraevens, K. (2022). Characterizing groundwater heat transport in a complex lowland aquifer using paleo-temperature reconstruction, satellite data, temperature depth profiles, and numerical models. *Hydrology and Earth System Sciences* 26(21), 5577–5604. <https://doi.org/10.5194/hess-26-5577-2022>
- Folmer, I., van Steijn, T., Holsteijn, A.-L., & Krikken, A. (2018a, April 9). Gebiedsdossier grondwaterwinning Herveldse veld. Royal Haskoning DHV.
- Folmer, I., van Steijn, T., Holsteijn, A.-L., & Krikken, A. (2018b, April 9). Gebiedsdossier grondwaterwinning La Cabine. Royal Haskoning DHV.
- Gumm, L. P., Bense, V. F., Dennis, P. F., Hiscock, K. M., Cremer, N., & Simon, S. (2016). Dissolved noble gases and stable isotopes as tracers of preferential fluid flow along faults in the Lower Rhine Embayment, Germany. *Hydrogeology Journal* 24(1), 99–108. <https://doi.org/10.1007/s10040-015-1321-7>
- Harris, R. N., & Chapman, D. S. (2007). Stop-go temperature logging for precision applications. *Geophysics* 72(4), E119–E123. <https://doi.org/10.1190/1.2734382>
- Hug, S. J., Winkel, L. H. E., Voegelin, A., Berg, M., & Johnson, A. C. (2020). Arsenic and Other Geogenic Contaminants in Groundwater – A Global Challenge. *CHIMIA*, 74(7), 524. <https://doi.org/10.2533/chimia.2020.524>
- J B, J., & Joseph, S. (2023). Sources of Groundwater Contamination: A Review. *International journal of research and review* <https://doi.org/10.52403/ijrr.20231016>

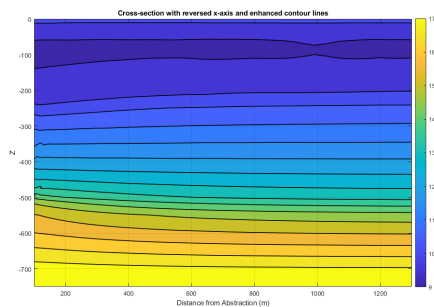
- Jasechko, S. (2019). Global Isotope Hydrogeology Review. *Reviews of Geophysics* 57(3), 835-965. <https://doi.org/10.1029/2018RG000627>
- Kurylyk, B. L., Irvine, D. J., & Bense, V. F. (2019). Theory, tools, and multidisciplinary applications for tracing groundwater fluxes from temperature profiles. *WIREs Water* 6(1), e1329. <https://doi.org/10.1002/wat2.1329>
- Kurylyk, B. L., & MacQuarrie, K. T. B. (2014). A new analytical solution for assessing climate change impacts on subsurface temperature. *Hydrological Processes* 28(7), 3161-3172. <https://doi.org/10.1002/hyp.9861>
- Lijzen, J. P. A., Otte, P., & van Dreumel, M. (2014). Towards sustainable management of groundwater: Policy developments in The Netherlands. *Science of The Total Environment* 485-486, 804-809. <https://doi.org/10.1016/j.scitotenv.2014.02.081>
- Pradhan, B., Chand, S., Chand, S., Rout, P. R., & Naik, S. K. (2023). Emerging groundwater contaminants: A comprehensive review on their health hazards and remediation technologies. *Groundwater for Sustainable Development* 20, 100868. <https://doi.org/10.1016/j.gsd.2022.100868>
- RWE. (n.d.). Hambach mine site | RWE. Retrieved September 9, 2024, from <https://www.rwe.com/en/the-group/countries-and-locations/hambach-mine-site/>
- Scanlon, B. R., Keese, K. E., Flint, A. L., Flint, L. E., Gaye, C. B., Edmunds, W. M., & Simmers, I. (2006). Global synthesis of groundwater recharge in semiarid and arid regions. *Hydrological Processes* 20(15), 3335-3370. <https://doi.org/10.1002/hyp.6335>
- Schäfer, A., Hilger, D., Gross, G., & von der Hocht, F. (1996). Cyclic sedimentation in Tertiary Lower-Rhine Basin (Germany) the 'Liegendrücken' of the brown-coal open-cast Fortuna mine. *Sedimentary Geology* 103(3), 229-247. [https://doi.org/10.1016/0037-0738\(95\)00091-7](https://doi.org/10.1016/0037-0738(95)00091-7)
- Shaji, E., Santosh, M., Sarath, K., Prakash, P., Deepchand, V., & Divya, B. (2021). Arsenic contamination of groundwater: A global synopsis with focus on the Indian Peninsula. *Geoscience Frontiers*, 12(3), 101079. <https://doi.org/10.1016/j.gsf.2020.08.015>
- Solutions, P. (n.d.). FlexPDE Modeling Software Tool - Partial Differential Equations [PDE solutions]. Retrieved September 19, 2024, from <https://www.pdesolutions.com/expde/>
- Taniguchi, M., Shimada, J., Tanaka, T., Kayane, I., Sakura, Y., Shimano, Y., Dapaah-Siakwan, S., & Kawashima, S. (1999). Disturbances of temperature-depth profiles due to surface climate change and subsurface water flow: 1. An effect of linear increase in surface temperature caused by global warming and urbanization in the Tokyo Metropolitan Area, Japan. *Water Resources Research* 35(5), 1507-1517. <https://doi.org/10.1029/1999WR900009>
- Thaw, M., GebreEgziabher, M., Villafañe-Pagán, J. Y., & Jasechko, S. (2022). Modern groundwater reaches deeper depths in heavily pumped aquifer systems. *Nature Communications*, 13(1), 5263. <https://doi.org/10.1038/s41467-022-32954-1>
- TNO. (2024). BRO REGIS II v2.2.2. TNO - Geologische Dienst Nederland. Retrieved January 23, 2025, from <https://www.dinoloket.nl/ondergrondmodellen/kaart>
- van Driezum, I., Beekman, J., van Loon, A., van Leerdam, R., Wuijts, S., Rutgers, M., Boekhold, S., & Zijp, M. (2020). Staat Drinkwaterbronnen RIVM. <https://doi.org/10.21945/RIVM-2020-0179>
- Vermeulen, P. T. M., te Stroet, C. B. M., & Heemink, A. W. (2006). Limitations to upscaling of groundwater flow models dominated by surface water interaction. *Water Resources Research* 42(10). <https://doi.org/10.1029/2005WR004620>
- Wada, Y., van Beek, L. P. H., van Kempen, C. M., Reckman, J. W. T. M., Vasak, S., & Bierkens, M. F. P. (2010). Global depletion of groundwater resources. *Geophysical Research Letters*, 37(20). <https://doi.org/10.1029/2010GL044571>
- Witte, H., Gelder, G., & Spittler, J. (2002). In Situ Measurement of Ground Thermal Conductivity: The Dutch Perspective. *ASHRAE Transactions* 108, 263-272.
- Wu, P., Comte, J.-C., Ma, Z., Li, F., & Chen, H. (2023). Scaling of groundwater flow subject to managed aquifer recharge using injection boreholes: Physical experiments and upscaled numerical

models. *Urban Climate*, 51, 101651. <https://doi.org/10.1016/j.uclim.2023.101651>

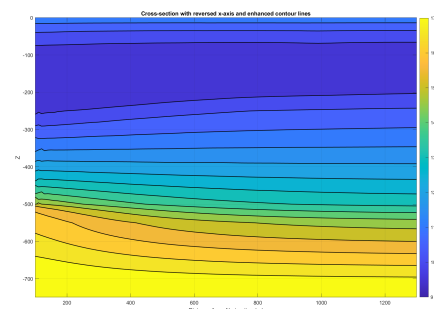
Ziagos, J. P., & Blackwell, D. D. (1986). A model for the transient temperature effects of horizontal fluid flow in geothermal systems. *Journal of Volcanology and Geothermal Research*, 27(3), 371–397. [https://doi.org/10.1016/0377-0273\(86\)90021-1](https://doi.org/10.1016/0377-0273(86)90021-1)



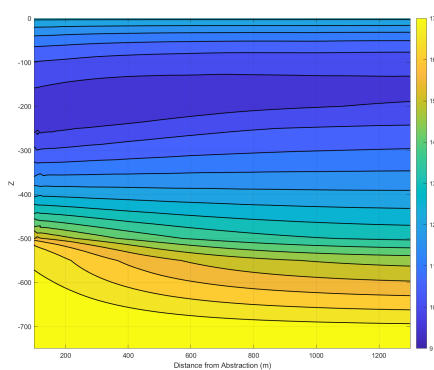
# A | Additional figures



(a)

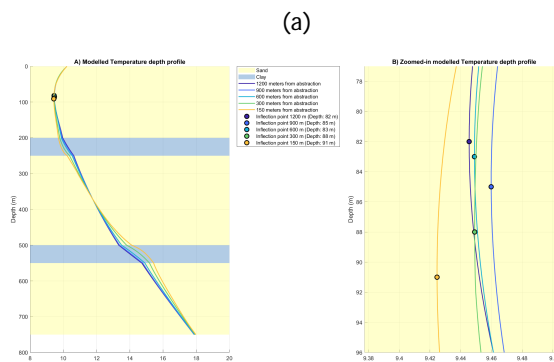


(b)

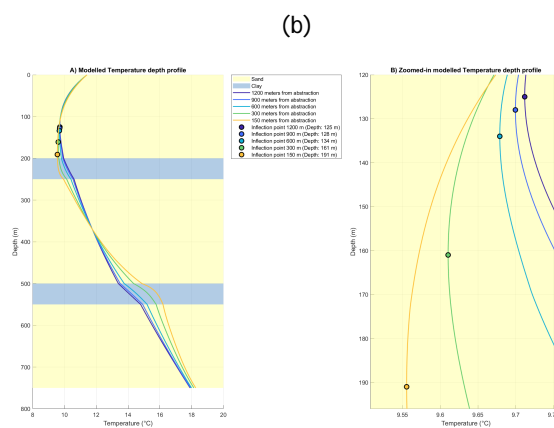


(c)

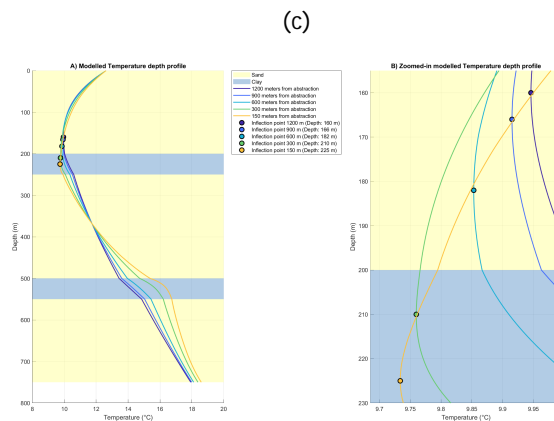
Figure A.1: Modelled temperature crosssections after 40, 100 and 160 years of abstraction. Near the abstraction site the largest differences can be observed



(a)



(b)



(c)

Figure A.2: Temperature depth profiles taken from the model at different distances from the abstraction site. On the left panes, the whole temperature-depth profile is plotted with different distances to the abstraction site. The right panel shows only the depths where the inflection points are located. Figure A is 40 years since abstraction, figure B is 100 years since abstraction, and figure C is 160 years since abstraction.

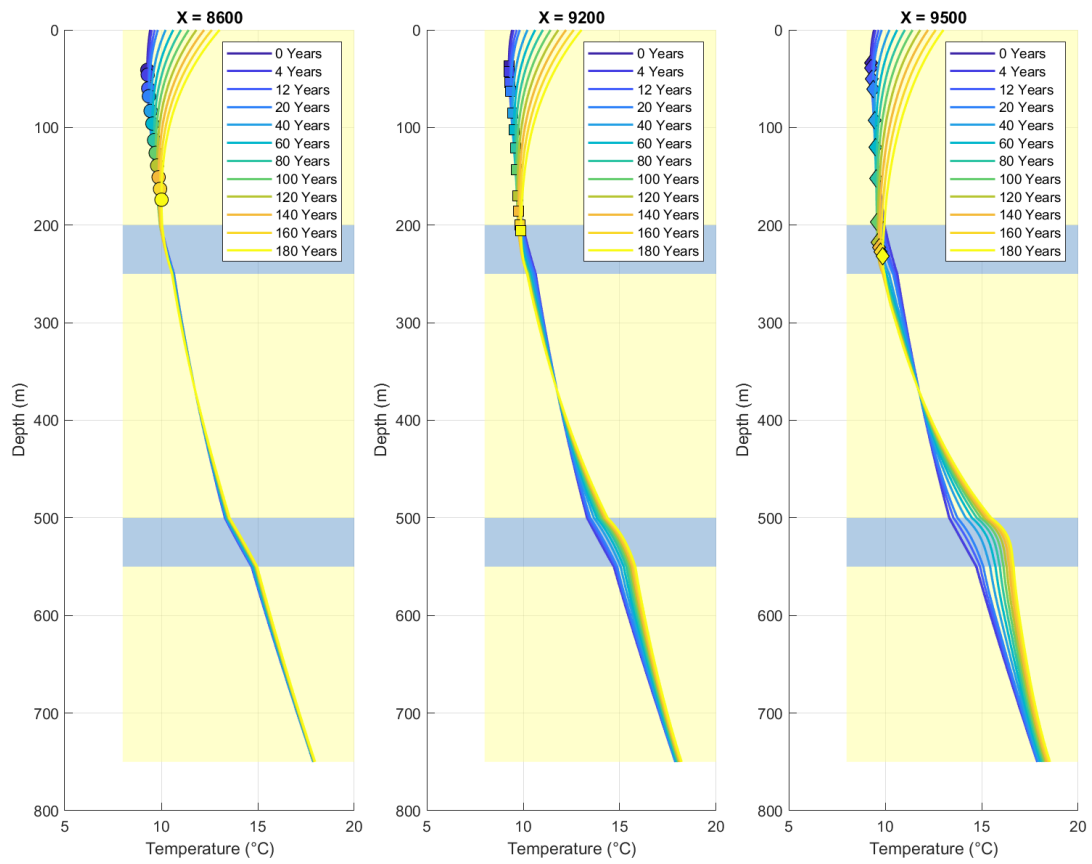


Figure A.3: The depth of the modelled inflection point over time, for the scenario with the increased head difference.. In yellow the inflection points 300 metres from abstraction are shown, in red 600 metres and in blue 1200 metres.

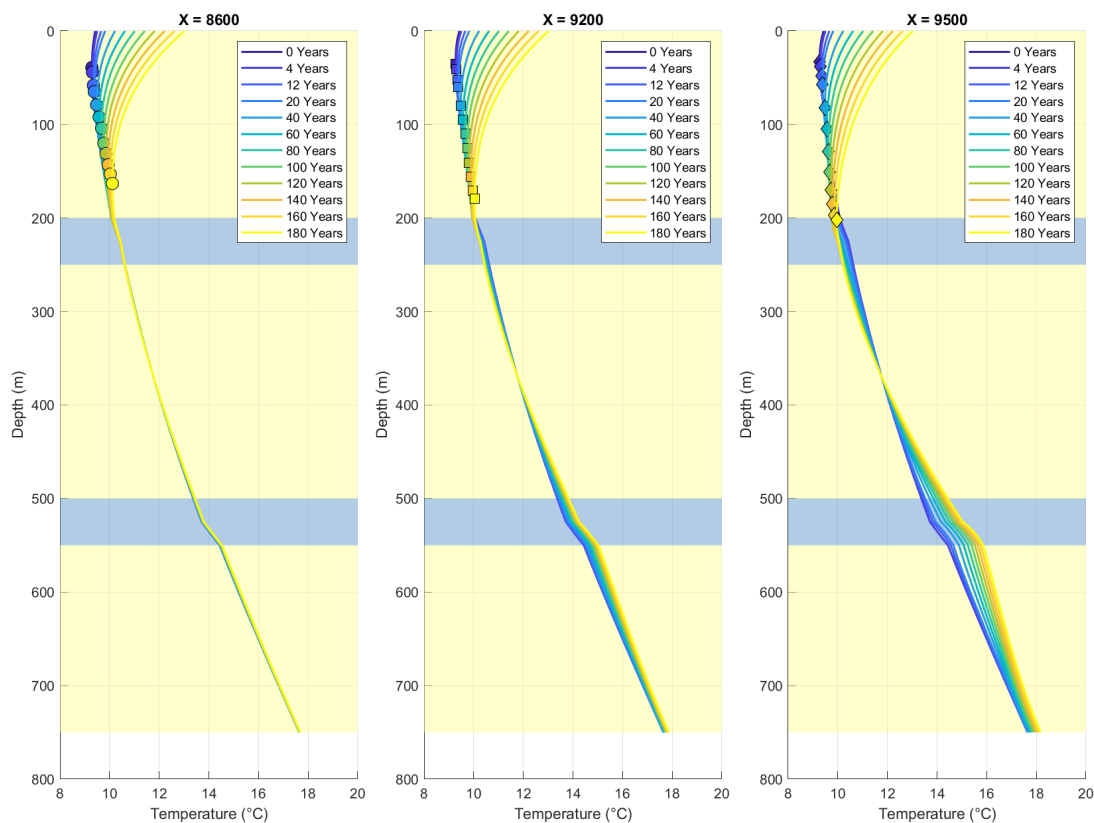


Figure A.4: The depth of the modelled inflection point over time, for the scenario with the decreased head difference. In yellow the inflection points 300 metres from abstraction are shown, in red 600 metres and in blue 1200 metres.

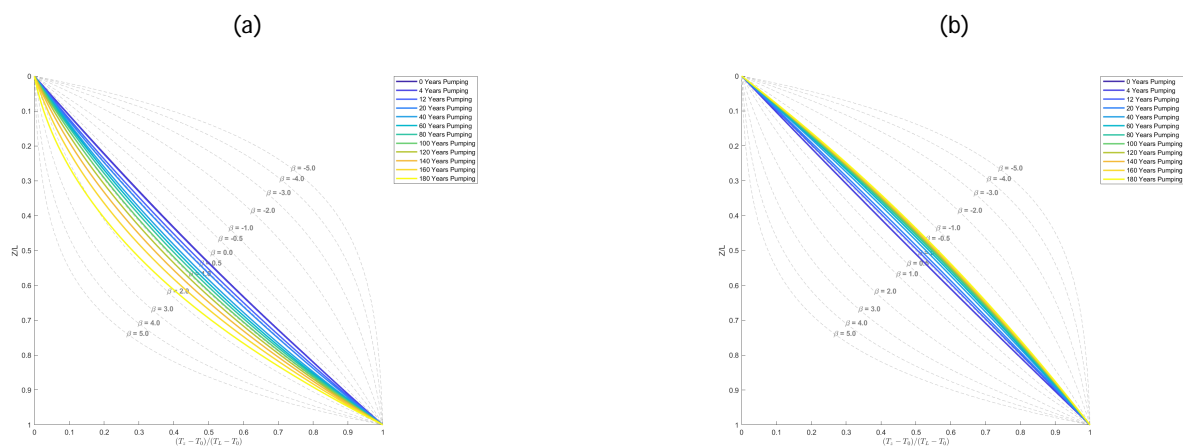


Figure A.5: Bredehoft curves for the shallow (figure A) and deep (figure B) aquitard at 600 metres from the abstraction site. The different times since abstraction are indicated with different colours.

